Biosci. Rep. (2012) / **32** / 443–453 (Printed in Great Britain) / doi 10.1042/BSR20120048

online data

Original Paper

Bioscience Reports

www.bioscirep.org

Bioscience Reports

Conformations of the apo-, substrate-bound and phosphate-bound ATP-binding domain of the Cu(II) ATPase CopB illustrate coupling of domain movement to the catalytic cycle

Samuel JAYAKANTHAN*, Sue A. ROBERTS*, Andrzej WEICHSEL*, José M. ARGÜELLO† and Megan M. McEVOY*‡[1]

*Department of Chemistry and Biochemistry, University of Arizona, Tucson, AZ 85721, U.S.A., ‡Department of Soil, Water and Environmental Science, University of Arizona, Tucson, AZ 85721, U.S.A., and †Department of Chemistry and Biochemistry, Worcester Polytechnic Institute, 100 Institute Road, Worcester, MA 01609, U.S.A.

Synopsis

Heavy metal P_{1B}-type ATPases play a critical role in cell survival by maintaining appropriate intracellular metal concentrations. *Archaeoglobus fulgidus* CopB is a member of this family that transports Cu(II) from the cytoplasm to the exterior of the cell using ATP as energy source. CopB has a 264 amino acid ATPBD (ATP-binding domain) that is essential for ATP binding and hydrolysis as well as ultimately transducing the energy to the transmembrane metal-binding site for metal occlusion and export. The relevant conformations of this domain during the different steps of the catalytic cycle are still under discussion. Through crystal structures of the apo- and phosphate-bound ATPBDs, with limited proteolysis and fluorescence studies of the apo- and substrate-bound states, we show that the isolated ATPBD of CopB cycles from an open conformation in the apo-state to a closed conformation in the substrate-bound state, then returns to an open conformation suitable for product release. The present work is the first structural report of an ATPBD with its physiologically relevant product (phosphate) bound. The solution studies we have performed help resolve questions on the potential influence of crystal packing on domain conformation. These results explain how phosphate is co-ordinated in ATPase transporters and give an insight into the physiologically relevant conformation of the ATPBD at different steps of the catalytic cycle.

Key words: ATPase transporter, ATP-binding domain (ATPBD), CopB, copper, crystal structure, metal transport.

Cite this article as: Jayakanthan, S., Roberts, S.A., Weichsel, A., Argüello, J.M., and McEvoy, M.M. (2012) Conformations of the apo-, substrate-bound and phosphate-bound ATP-binding domain of the Cu(II) ATPase CopB illustrate coupling of domain movement to the catalytic. Biosci. Rep. **32**, 443–453

INTRODUCTION

P-type ATPases are transmembrane proteins involved in the active transport of charged ions across the cell membrane driven by the hydrolysis of ATP [1]. With different substrate specificities, these enzymes aid in processes such as action potential, relaxation of muscle tissues and signal transduction [2,3]. P_{1B}-ATPases are a subgroup of P-type ATPases that play an important role in metal homoeostasis selectively transporting heavy metals such as Cu(I), Cu(II), Zn(II) and Co(II) across the biological membranes [4,5]. These transporters confer metal tolerance to bacteria and aid in metal efflux from the cytoplasm. In eukaryotes, they play a role in metal micronutrient absorption, distribution and clearance [6–12].

Studies on full-length transporters as well as individual domains have helped define the major structural characteristics of P-type ATPases. These enzymes generally contain six to ten

Abbreviations used: A-domain, actuator domain; AMPPCP, adenosine 5′-(β,γ-methylene)triphosphate; ATPBD; ATP-binding domain; HAD; haloacid dehalogenase; IPTG, isopropyl β-D-thiogalactoside; Lp-CopA, *Legionella pneumophila* CopA; MBD, metal-binding domain; N-domain, nucleotide-binding domain; p[NH]ppA, adenosine 5′-[β,γ-imido]triphosphate; PEG, poly(ethylene glycol); P-domain, phosphorylation doamin; RMSD, root mean square deviation; SERCA1, sarcoplasmic/endoplasmic reticulum Ca^{2+}-ATPase 1; SSRL, Stanford Synchrotron Radiation Lightsource.

[1] To whom correspondence should be addressed at the present address: Department of Chemistry and Biochemistry, University of Arizona, Tucson, AZ 85721, U.S.A. (email mcevoy@email.arizona.edu).

The atomic co-ordinates and the structure factors of the apo- and phosphate-bound ATPBD of *Archaeoglobus fulgidus* CopB crystallized in space group $P22_12_1$ will appear in the PDB under accession codes 3SKX and 3SKY respectively.

transmembrane α-helices (H1–H10) and two to three cytosolic domains that play a role in ATP hydrolysis and ligand-dependent regulation of transport. The cytosolic ATPBD (ATP-binding domain) functions in ATP-binding, hydrolysis and subsequent transfer of energy for ion transport. The A-domain (actuator domain) aids in the catalytic cycle by making transient interactions with the ATPBD and the MBDs (metal-binding domains) [4,13]. All P_{1B}-ATPases have anywhere from one to six MBDs at the N-terminal end of the protein sequence, with the exception of a few enzymes that have a C-terminal metal-binding motif [9,14,15]. MBDs have been shown to play a crucial role in the transport process by co-ordinating metal ions selectively either from the cytosol or from chaperones, and transferring them to the transmembrane metal-binding site via transient inter-domain interactions with the ATPBD and A-domain [4,9,15,16].

The P_{1B}-ATPases follow the classical E1/E2 Albers-Post catalytic cycle to transport metals across membranes. The catalytic activity takes place in the ATPBD, which binds and hydrolyses ATP resulting in the phosphorylation of an aspartate in the highly conserved DKTGT segment of the domain [4]. This transport mechanism has been extensively characterized structurally in the Na^+, K^+, Ca^{2+} and H^+, K^+-ATPases where enzyme phosphorylation occurs upon ATP-binding to the ATPBD and metal binding to the transmembrane metal-binding site from the cytoplasmic side [13,17–20]. Movement of domains and intradomain conformation changes are clearly important for the function of these enzymes. Structural studies of P_2-type ATPases indicate rigid body movements of the ATPBD during the catalytic cycle, where it makes transient domain–domain interactions with other cytosolic domains [21]. These transient domain–domain interactions are postulated to play a crucial role in facilitating the transport cycle [22].

Previous structural and functional studies on isolated ATPBDs from archaea and humans have demonstrated that the isolated domains are soluble and retain the ability to bind and hydrolyse ATP [23–25]. The three-dimensional structures of apo- and nucleotide-bound ATPBDs of some well-characterized Cu(I)-transporting ATPases such as CopA (*Archaeoglobus fulgidus*), CopB (*Sulfolobus solfataricus*) and the N-domain (nucleotide-binding domain) of the Wilson's disease protein (*Homo sapiens*) clearly revealed the nucleotide-binding mechanism and phosphorylation regions [23–28]. More recently, the structure of the full-length Cu(I) transporter CopA from *Legionella pneumophila* (Lp-CopA) was solved at a resolution of 3.2 Å resolution in a copper-free/nucleotide-free form [29].

Copper homoeostasis in the extreme thermophile *A. fulgidus* is maintained by the two P_{1B}-ATPases: the Cu(I)-transporting CopA and the Cu(II)-transporting CopB [8,9]. Although *A. fulgidus* CopA has been extensively characterized, the Cu(II)-transporting ATPase CopB has not been as well studied. The previous work on CopB showed that the ATPase is active at 75 °C and has high ionic strength in the presence of Cu(II) [9]. That study also attributed the Cu(II) selectivity of this ATPase to a histidine residue of the CPH sequence in the sixth transmembrane segment. The histidine-rich N-terminal MBD was found to play a regulatory role in metal transport by influencing the rate of dephosphorylation [9].

In *A. fulgidus* CopB the 264 amino acid ATPBD is located between transmembrane helices H6 and H7 on the cytosolic side of the membrane. The ATPBD is comprised of two domains: the P-domain (phosphorylation domain), which contains the site of phosphorylation, Asp^{389}, within the conserved sequence DKTGT, and the N-domain (nucleotide-binding domain) that binds and hydrolyses ATP.

In the present paper, we provide structural and biochemical characterization of the ATPBD of the Cu(II)-transporting CopB from *A. fulgidus*. We have demonstrated that the isolated domain is active at 75 °C and has affinity for ATP in the low micromolar range. We have determined the structures of the isolated domain in both the apo form and the phosphate ion-bound form, which were both found to be in open conformation. To the best of our knowledge, this is the only structure of the ATPBD in its open conformation with a physiological/endogenous ligand in its active site. Using limited proteolysis and fluorescence assays, we have also shown that the domain undergoes ligand-induced conformational changes. These studies bring new insights to our understanding of how these transporters function in the cell.

EXPERIMENTAL

Chemicals

All chemicals were obtained from Sigma–Aldrich, unless otherwise noted, and were of reagent grade or better.

Purification of the ATPBD from *A. fulgidus* CopB

The DNA region encoding the ATPBD from *A. fulgidus* CopB (residues Arg^{372}–Lys^{636}) was PCR-amplified using pfu turbo DNA polymerase (Stratagene) from a plasmid containing the gene of the full-length enzyme using the nucleotide primer pair 5′-CCCTCTAGAAATAATTTTGTTTAACTTTAAGAAGGAGATATACAAATGAGGGACAGGCAGGCCT-3′ and 5′-AAACCATGGAACTTCGAGTAGGTTTTTCTT-3′ (IDT). The resulting fragment was purified using the QIAquick PCR purification kit (Qiagen), digested with XbaI and NcoI (New England Biolabs), and ligated into a pPR-IBAI vector (IBA), which introduces a Strep-tactin tag (WSHPQFEK) at the C-terminus of the protein, creating plasmid $4ATPBD_{372–636}$. The construct was sequenced and verified for accuracy (UAGC, University of Arizona). The protein expressed from this construct was used for all experiments in this paper except for the phosphate-bound structure, which was used in the His-tagged construct described below.

The plasmid $4ATPBD_{372–636}$ was transformed into *Escherichia coli* Rosetta cells (Invitrogen). The cells were grown at 37 °C in 2×YT medium supplemented with 100 μg/ml ampicillin and 34 μg/ml chloramphenicol. At mid-log protein expression was induced with 1 mM IPTG (isopropyl β-D-thiogalactoside).

The cells were harvested by centrifugation at 6 h post-induction, washed with buffer W containing 100 mM Tris/HCl (pH 8.0) and 150 mM NaCl, and treated with a cocktail of protease inhibitors (leupeptin, pepstatin A and 1 mM PMSF) and DNase (with 5 mM $MgCl_2$).

The resuspended cell solution was lysed by French press and centrifuged at 163 000 ***g*** for 1 h. The supernatant was loaded on to a 10 ml streptactin column (IBA) equilibrated with 10 column volumes of buffer W. After washing the column with 5 column volumes of buffer W the protein was eluted with a buffer W containing 2.5 mM desthiobiotin. Aliquots of fractions were separated by SDS/PAGE, which was stained with Coomassie Blue. Those fractions judged to be greater than 95% pure were pooled and concentrated for further use. Maximum yields were ~10 mg/l.

A selenomethionine derivative of the ATPBD from *A. fulgidus* CopB was prepared by growing *E. coli* Rosetta (Invitrogen) cells in an M9 minimal medium at 37 °C with 100 μg/ml ampicillin. When the cells reached a D_{600} of ~0.3, 100 mg of L-lysine, 100 mg of L-phenylalanine, 100 mg of L-threonine, 50 mg of L-isoleucine, 50 mg of L-leucine, 50 mg of L-valine and 50 mg of L-selenomethionine were added per litre of culture. The cells were induced after 15 min with 1 mM IPTG and were harvested after 5 h. Purification was performed as described above for the native protein.

The pET system [pET22b(+)] (Novagen) was used to create a construct expressing the ATPBD with a C-terminal His-tag. The gene corresponding to the ATPBD was amplified using the nucleotide primer pair 5′-GGAATTCCATATGAGGGACAGGCAGGCCTTCGAGAGG-3′ and 5′-GTCCGCTCGAGCTTCGAGTAGGTTTTTCTTGATAGC-3′ (IDT). The resulting fragment was purified using the QIAquick PCR purification kit (Qiagen) prior to digestion with NdeI and XhoI (New England Biolabs). The resulting plasmid *ATPBDH* encodes a His_6 tag at the C-terminus of the fragment. Cell growth and protein expression were performed as described above. Purification of Ni-NTA (Ni^{2+}-nitrilotriacetate) resin was performed according to the manufacturer's recommendations (GE Healthcare). Maximum yields were ~20 mg/l. Protein from this preparation was used for the determination of the phosphate anion-bound structure.

Characterization of ATPBD using far-UV CD

Purified Strep-tagged protein sample was exchanged in a buffer containing 25 mM Hepes, 100 mM NaCl (pH 6.5). Far-UV CD wavelength scans were acquired with ~8 μM protein in a 0.1 mm path-length cuvette using an Olis DSM CD spectrometer. Percentage helicity was calculated by using $100\times([\theta]_{222}/^{\max}[\theta]_{222})$, where $^{\max}[\theta]_{222} = -35481.2121\times[1-(2.5/n)]$, $n = 264$ amino acids and $[\theta]_{222} = -116.76$. A temperature melt performed from 20 to 80 °C was followed by the acquisition of a secondary structure scan.

Site-directed mutagenesis

Site-directed mutagenesis to produce the mutant E422A was performed using a QuikChange™ site-directed mutagenesis kit (Stratagene), using the nucleotide primer pair 5′-TCGCCGCATCCCTCGCTGCGAGGTCTGAGCAT-3′ and 5′-ATGCTCAGACCTCGCAGCGAGGGATGCGGCGA-3′ (IDT). The alteration was confirmed by automated DNA sequencing (University of Arizona Genetics Core, University of Arizona, Tucson, AZ, U.S.A.). Cell growth, protein expression and protein purification were carried out as described for the wild-type protein.

ATPase activity

Activity assays were carried out using a 300 μl of solution containing 20 μM ATPBD in 50 mM Tris/HCl (pH 7.5) and 50 mM NaCl to which 50 μl of ATPase mix (1 mM $MgCl_2$ and 5 mM ATP) was added. The reaction was initiated by placing the reaction mixture in a 75 °C water bath. After incubating for 10 min, the reaction was stopped by quickly cooling the solution to 4 °C. A control reaction was performed without the enzyme. The free phosphate concentration was measured at room temperature (25 °C) by using the EnzChek phosphate assay kit (Molecular Probes). As an additional control, the reactions were also performed at room temperature.

Crystallization and structure determination of the apo-ATPBD from *A. fulgidus* CopB

The purified protein was exchanged into 20 mM Mops (pH 7.0), 20 mM NaCl and 5% (v/v) glycerol using a Sephacryl S-200 gel filtration column and was concentrated to 25 mg/ml. The concentrated protein was flash frozen in liquid nitrogen and stored at −80 °C.

Crystals of both ATPBD and selenomethionine–ATPBD were grown by the hanging drop vapour diffusion method. A portion (2 μl) of protein solution was mixed with 2 μl of a precipitant solution containing 0.2 M sodium acetate, 0.1 M Tris/HCl (pH 8.5), 22% (w/v) PEG [poly(ethylene glycol)] 4000 and 0.01 M magnesium chloride, and equilibrated against the precipitant solution. Rectangular (native) or rod-shaped crystals (selenomethionine-substituted protein) were obtained.

The crystals were transferred to a solution enriched to 36% PEG4000 and flash frozen in liquid nitrogen. Diffraction images were obtained remotely at Beam line 9-2 at the SSRL (Stanford Synchrotron Radiation Lightsource). MAD data were collected at three wavelengths from a selenomethionine-substituted crystal. All the data were processed and scaled using CrystalClear [30]. The structure was determined using MAD phasing of data for the selenomethionine-labelled protein. Four of the five expected selenium positions were found by and initial phasing performed using SOLVE (v 2.08) [31]. Density modification was performed using RESOLVE [31]. The initial structural model, 255 residues, was autobuilt using RESOLVE and BUCCANEER [32]. This structure was then used as a starting model for the native data set. The structure was refined using Refmac5 [33] with manual rebuilding using COOT [34]. Data collection, phasing and refinement statistics are shown in Table 1.

Table 1 Crystallographic data collection and refinement for apo-ATPBD of *A. fulgidus* CopB
Values in the wavelength, resolution, total/unique reflections, completeness, mean I/σ and R_{merge} rows of the selenomethionine derviative are for the peak, remote, inflection.

Parameter	Selenomethionine derviative	Native
Crystal class	Orthorhombic	Orthorhombic
Space group	$P22_12_1$	$P22_12_1$
Cell parameters (Å)	$a=36.58$, $b=63.24$, $c=106.15$	$a=36.05$, $b=62.68$, $c=106.06$
Z (molecules/au)	1	1
Temperature (K)	100	100
Wavelength (Å)	0.9792, 0.9116, 0.9793	0.9792
Resolution (Å)	1.90, 1.90, 1.90	1.59
Total/unique reflections	153302/35918, 153279/35862, 154606/36038	177340/31479
Completeness (%)*	95/93, 95/90, 95/90	95/93
Mean $I/\sigma(I)$*	18.3/4.4, 18.4/5.1, 19.3/5.0	25.0/4.9
R_{merge}*†	0.039/0.20, 0.037/0.21, 0.034/0.22	0.033/0.24
FOM (solve)	0.40–1.90 Å	
R_{cryst}/R_{free}‡		0.20/0.23
RMSD bonds (Å)/angles (°)		0.010/1.2
Residues in most favourable/additional allowed regions of Ramachandran plot (%)		93.9/5.7
Avg B (Å^2)		24.0

*Overall/outermost shell.
†$R_{merge}=\Sigma hkl\ \Sigma i|Ii(hkl)-<I(hkl)>|/\Sigma hkl\ \Sigma i\ I(hkl)$, where $<I(hkl)>$ is the mean intensity of all symmetry-related reflections $Ii(hkl)$.
‡$R_{cryst}=(|\Sigma F_{obs}-F_{calc}|)/\Sigma F_{obs}$; R_{free} as for R_{cryst}, using a random subset of the data (5%) not included in the refinement.

Crystallization and structure determination of the phosphate-bound ATPBD from *A. fulgidus* CopB

The purified ATPBD (25 mg/ml) was thawed on ice followed by the addition of 2 mM p[NH]ppA (adenosine 5′-[β,γ-imido]triphosphate) and 3 mM $MgCl_2$. The crystals were grown by the hanging-drop method. Equal volumes of protein and a precipitant solution containing 0.2 M ammonium acetate, 0.1 M Hepes pH 7.5, 25% PEG 3350 were mixed and equilibrated against the precipitant solution. Large rectangular crystals grew within 2–3 weeks. A rectangular crystal was quickly exchanged into a cryosolvent containing 0.1 M Hepes (pH 7.5) and 35% PEG3350 and was flash frozen in liquid nitrogen. Data were measured at SSRL. The crystals belonged to the space group $P22_12_1$ with one molecule in the asymmetric unit. The apo-ATPBD structure was used as a starting model. The structure was refined using Refmac5 [33] with manual rebuilding using COOT [34]. Data measurement, phasing and refinement statistics are given in Table 2. Co-ordinates and structure factors for both the apo- and anion-bound structures have been deposited in the PDB, accession numbers 3SKX (apo-ATPBD) and 3SKY (phosphate-bound ATPBD).

Table 2 Crystallographic data collection and refinement for phosphate-bound ATPBD of *A. fulgidus* CopB

Parameter	Phosphate-bound native ATPBD
Crystal class	Orthorhombic
Space group	$P22_12_1$
Cell parameters (Å)	$a=35.76$ $b=62.91$ $c=106.54$
Z (molecules/au)	1
Temperature (K)	100
Wavelength (Å)	0.9790
Resolution (Å)	2.10
Total/unique reflections	99848/14659
Completeness (%)*	99.6/98.0
Mean $I/\sigma(I)$*	18.7/4.8
R_{merge}*†	0.045/0.27
R_{cryst}/R_{free}‡	0.21/0.26
RMSD bonds (Å)/angles (°)	0.013/1.4
Residues in most favourable/additional allowed regions of Ramachandran plot (%)	94.7/5.3
Avg B (Å^2)	35.3

*Overall/outermost shell.
†$R_{merge}=\Sigma hkl\ \Sigma i|Ii(hkl)-<I(hkl)>|/\Sigma hkl\ \Sigma i\ I(hkl)$, where $<I(hkl)>$ is the mean intensity of all symmetry-related reflections $Ii(hkl)$.
‡$R_{cryst}=(|\Sigma F_{obs}-F_{calc}|)/\Sigma F_{obs}$; R_{free} as for R_{cryst}, using a random subset of the data (5%) not included in the refinement.

Limited proteolysis of ATPBD

Proteolysis was performed by adding 5 μg of trypsin (in 1 mM HCl) to 600 μl of 20 μM ATPBD in 50 mM Tris/HCl (pH 7.5) and 50 mM NaCl. The samples were incubated on ice. At 12 time points 50 μl aliquots were removed from the reaction mixture and added to a vial containing 10 μl of SDS/PAGE gel-loading dye, thereby quenching the reaction. Similar reactions were performed with the addition of 4 mM AMPPCP [adenosine 5′-(β,γ-methylene)triphosphate] (with 4 mM $MgCl_2$). The samples were run on a 12-well 4–20% gradient Pre-cast gel (Expedion).

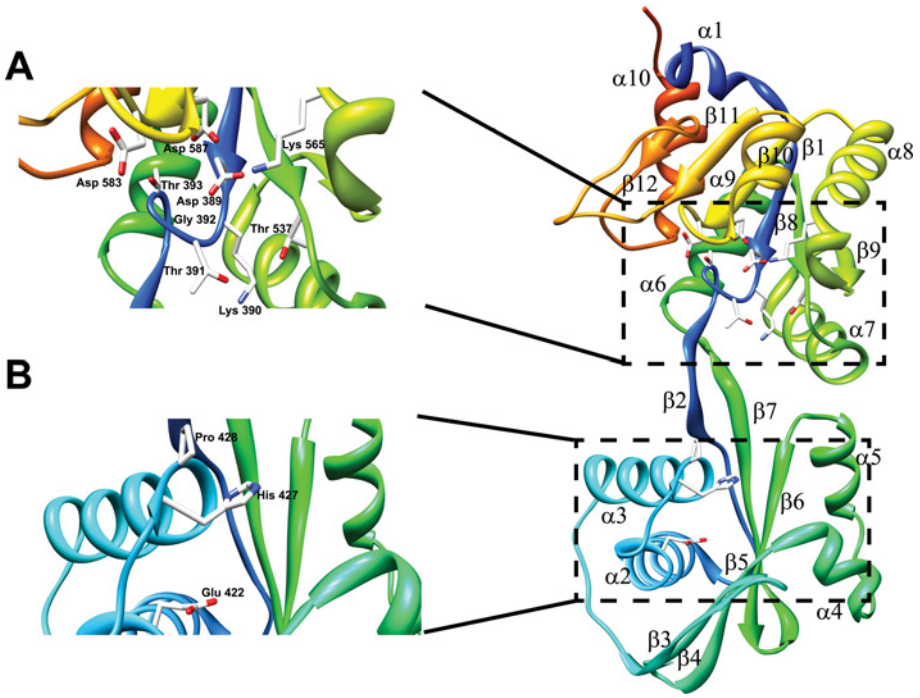

Figure 1 **Ribbon diagram of the apo-ATPBD of *A. fulgidus* CopB**
The highly conserved residues in the P- and N-domains are highlighted as sticks. The residues Asp[389], Gly[392] and Thr[393] form Motif I, whereas Thr[537] forms Motif II, and Lys[565], Asp[583] and Asp[587] form Motif III of the HAD super family. The secondary structural elements (α1–α10 and β1–β12) are annotated alongside the respective α-helices and β-strands. Ribbon diagrams were generated using UCSF Chimera [48].

The intensities of the respective bands of the full length and proteolysed fragments were quantified using ImageJ (NIH). The total intensities were calculated, plotted and fitted using SigmaPlot [35] (Systat Software).

Fluorescence assays

Fluorescence measurements were performed with 1 μM ATPBD in 50 mM Tris/HCl (pH 7.5) and 50 mM NaCl. ATP was freshly prepared in the same buffer and flash frozen to prevent hydrolysis. The fluorescence excitation wavelength was set to 280 nm and the emission was recorded from 290 to 420 nm on a Cary Eclipse Fluorimeter (Varian). The experiments were performed at room temperature to minimize turnover of ATP. Fluorescence due to ATP alone was found to be negligible. A titration was performed with a buffer alone to account for the change in fluorescence due to dilution, which was subsequently subtracted from the titration performed with the ligand. The data were analysed and plotted using SigmaPlot (Systat Software).

Solvent accessibility calculations for Trp[546]

The closed nucleotide-bound structure of *A. fulgidus* CopA ATPBD (PDB code 3A1C [25]) was used as a template to model CopB in the closed conformation using SWISS-MODEL [36]. The solvent accessible surface area for Trp[546] was calculated using the program AREAIMOL from the CCP4i suite of programs [37].

RESULTS AND DISCUSSION

CopB ATPBD structure

The ATPBD of *A. fulgidus* CopB plays a central role in the catalytic cycle by coupling enzyme phosphorylation to metal transport. The isolated ATPBD of CopB was examined for folding and function using CD and activity assays. Far-UV CD spectra of the ATPBD showed a profile characteristic of a well-folded protein with minima at 208 and 222 nm (Supplementary Figure S1A at http://www.bioscirep.org/bsr/032/bsr0320443add.htm), from which the percentage helicity is estimated to be 35%. A temperature melt of the ATPBD showed cooperative melting behaviour with a T_m of 60°C (Supplementary Figure S1B), although unfolding was not completely reversible (Supplementary Figure S1A). The isolated ATPBD exhibited activity at 75°C (354 ± 70 nmol of P_i/mg per min) consistent with that seen with the isolated ATPBD domain of CopA from the same organism [25]. When Glu[422], which is involved in ATP binding in homologues [28], was mutated to alanine, the ATPase activity

significantly decreased (15 ± 7 nmol of P_i/mg per min). Together, these studies indicate that the isolated ATPBD of CopB is folded and functional.

The 1.6 Å resolution crystal structure of the ATPBD of *A. fulgidus* CopB was determined using MAD phasing from a selenomethionine derivative. Similar to the structures of ATPBDs of other known P-type ATPases, the *A. fulgidus* CopB ATPBD has a kidney bean-like topology in which the P- and N-domains are separated by two short loops (Figure 1). The CopB ATPBD is structurally very similar to the ATPBD of CopA from the same organism (PDB code 2B8E [25]) with an overall RMSD (root mean square deviation) of 0.9 Å. Structural comparisons of the CopB ATPBD with the ATPBDs of other well-characterized ATPases, such as Na^+, K^+, SERCA1 (sarcoplasmic/endoplasmic reticulum Ca^{2+}-ATPase 1), WND (Wilson disease protein) and Kdp, reveal that the archaeal ATPBD has fewer helices, strands and loops than the eukaryotic ATPBDs, particularly in the N-domain [17,27,38]. The eukaryotic ATPBDs possess several more secondary structural elements in addition to longer loop regions (10–50 residues long) [17,27,38]. These differences are apparent in the TOPS topology diagrams comparing the eukaryotic Ca(II) transporter SERCA1 and CopB ATPBDs (Supplementary Figure S2 at http://www.bioscirep.org/bsr/032/bsr0320443add.htm).

Nucleotide binding takes place in the N-domain, which is comprised of six antiparallel β-strands (strands $\beta2$–$\beta7$) flanked by two sets of α-helices ($\alpha2$–$\alpha3$ and $\alpha4$–$\alpha5$) (Figure 1). The overall fold of the CopB N-domain is very similar to its homologues in that it shares core secondary structural elements despite low sequence identity [17,20,38,39]. Multiple sequence alignment of five structurally characterized copper ATPases (Supplementary Figure S3 at http://www.bioscirep.org/bsr/032/bsr0320443add.htm) show that the nucleotide-binding cleft of CopB has the signature motif (Glu^{422}, His^{427}–Pro^{428}, Gly^{455} and Gly^{457}), which is highly conserved among P_{1B}-type ATPases (Figure 1). CopB ATPBD has some additional residues in β-strands 4 and 5, which result in a more elongated sheet than the one found in CopA. The conserved residues Glu^{422}, His^{427}–Pro^{428}, which stabilize ATP-binding by orienting the adenine ring via hydrogen bonding [28], are found near the ends of α-helices 2 and 3 (Figure 1).

The P-domain of CopB, which contains the phosphorylation site, has a six-stranded parallel β-sheet ($\beta1$, $\beta8$–$\beta12$) with three α-helices on each side of the sheet (Figure 1) in what resembles an imperfect Rossmann fold as described by CATH protein structure classification [40]. The phosphorylation site, Asp^{389}, is located within the invariant D^{389}KTGT and T^{537}GD sequences, which face the ATP-binding site of the N-domain (Figure 1). These sequences are part of the HAD (haloacid dehalogenase) superfamily (HAD motif) commonly seen in hydrolases [41]. Residues Asp^{389}, Gly^{392} and Thr^{393} form Motif I, Thr^{537} forms Motif II, and Lys^{565}, Asp^{583} and Asp^{587} form Motif III of the HAD superfamily.

In P-type ATPases, the P-domain interacts with the A-domain at different points in the catalytic cycle, as seen in the SERCA1 ATPase structures [17,42,43] and Lp-CopA structures [29]. The surface of the P-domain makes these interactions correspond to the region between $\beta11$ and $\beta12$ in the CopB structure. In

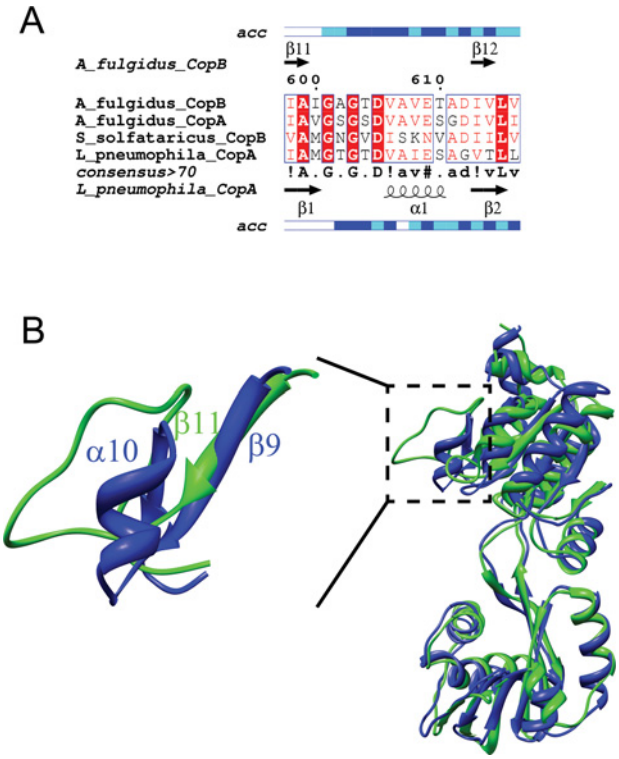

Figure 2 Secondary structure differences between the P-domains of CopB and Lp-CopA

(**A**) Multiple sequence alignment of the residues corresponding to the loop/helical segment in the P-domains whose structures are known. The secondary structural elements are displayed for CopB (top) and Lp–CopA (bottom). Sequence alignment was performed using CLUSTALW [49]. The solvent accessible residues for CopB (top) and Lp-CopA (bottom) are indicated by bars running parallel to the alignment with colours ranging from white to dark blue. The accessibility information is extracted from the corresponding DSSP file. Blue indicates accessible, cyan indicates intermediate, and white indicates that the residues are buried. This Figure was prepared using the Program ESPript [50]. (**B**). Cartoon models of CopB (green) and Lp-CopA (blue) superimposed with the insert highlighting the different secondary structure elements between the two structures. The structural alignment was performed using the structure comparison tool Matchmaker in the program UCSF Chimera. The ribbon diagram was generated using UCSF Chimera [48].

SERCA1 and Lp-CopA (Figure 2), where interdomain contacts are seen, this region is helical. In the CopB ATPBD (Figure 2), as well as the ATPBDs of *A. fulgidus* CopA [28] and *S. solfataricus* CopB [24], this region has an irregular loop conformation. It is possible that domain–domain interactions influence the structure in this region of the P-domain, and a helical structure potentially could be adopted when the A-domain is bound. Somewhat high B-factors in this region of the CopB ATPBD domain compared with the surrounding residues may reflect some structural flexibility.

Phosphate anion-binding site

The ATPBD of *A. fulgidus* CopB was co-crystallized with a nucleotide (p[NH]ppA). After accounting for the protein, the electron density showed a significant positive peak near

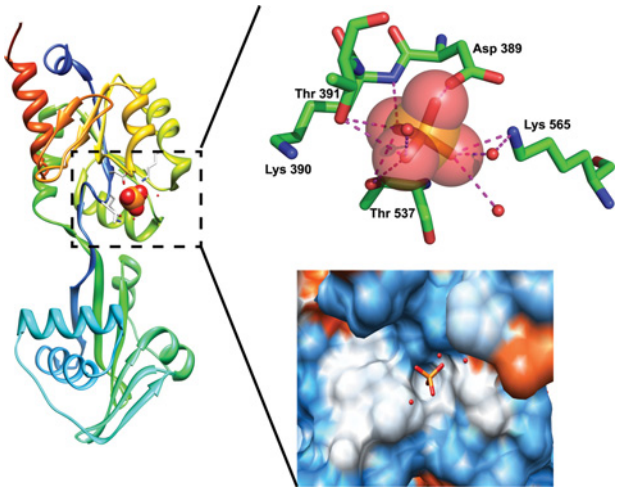

Figure 3 Ribbon representation of the 2.1 Å structure of *A. fulgidus* CopB ATPBD with bound phosphate

The insert shows the phosphate anion being stabilized by the conserved HAD motif residues Lys^{565}, Thr^{391}, Thr^{537}, Asp^{389} and two water molecules. The phosphate anion in the upper panel is displayed as orange and red spheres. The conserved residues are displayed as sticks. The surface diagram in the lower panel illustrates the surface charges on the anion binding pocket, with blue and red surfaces indicating positively and negatively charged surfaces. The anion is displayed as orange and red sticks, whereas the water molecules are displayed as red spheres. The Models were generated using Pymol and UCSF Chimera, respectively.

the expected nucleotide-binding site. Although this density was too small to accommodate the full nucleotide, a phosphate anion, one of the hydrolysis products of p[NH]ppA, fits very well into this feature with respect to size and chemical interactions with the protein (Figure 3, and Supplementary Figure S4 at http://www.bioscirep.org/bsr/032/bsr0320443add.htm). No other possible anions, such as sulfate, were present in the crystallization conditions or the protein purification buffers, supporting the identification of this feature as a phosphate anion.

In the catalytic cycle, the phosphate-bound ATPBD occurs in the transition from the E2-P state to the E2 state [4]. This state follows ATP hydrolysis to ADP and phosphorylation of Asp^{389}, then subsequent dissociation of ADP from the N-domain. The phosphate-bound ATPBD is obtained after cleavage of the covalently bound phosphate from Asp^{389}. Previously, several other structures of isolated and full-length ATPases with anions in the active site have been reported [24,29,43–45]. The phosphate-bound structure of *A. fulgidus* CopB is the only structure of a heavy metal ATPase with its physiologically relevant product bound to its active site.

The phosphate anion is located in a pocket in the P-domain bound to residues that are part of the HAD motif (Figure 3). The phosphate anion in CopB ATPBD is stabilized by hydrogen bonds with Lys^{565}, Thr^{391}, Thr^{537} and Asp^{389}. In addition there are hydrogen bonds from two water molecules and the backbone amide nitrogen of Lys^{390}. Although a divalent cation such as Mg(II) is a common feature in anion-binding sites of the HAD superfamily of proteins, the electron density at the anion-binding site of the CopB ATPBD did not have features to accommodate Mg(II) (Supplementary Figure S4). A few other previously reported structures of HAD superfamily proteins also lack Mg(II). For example, the ATPBD of CopB from *S. solfataricus* has a sulfate bound to the conserved HAD motif without divalent Mg(II) [24]. The HAD-containing cyanobacterial sucrose-phosphatase [46]

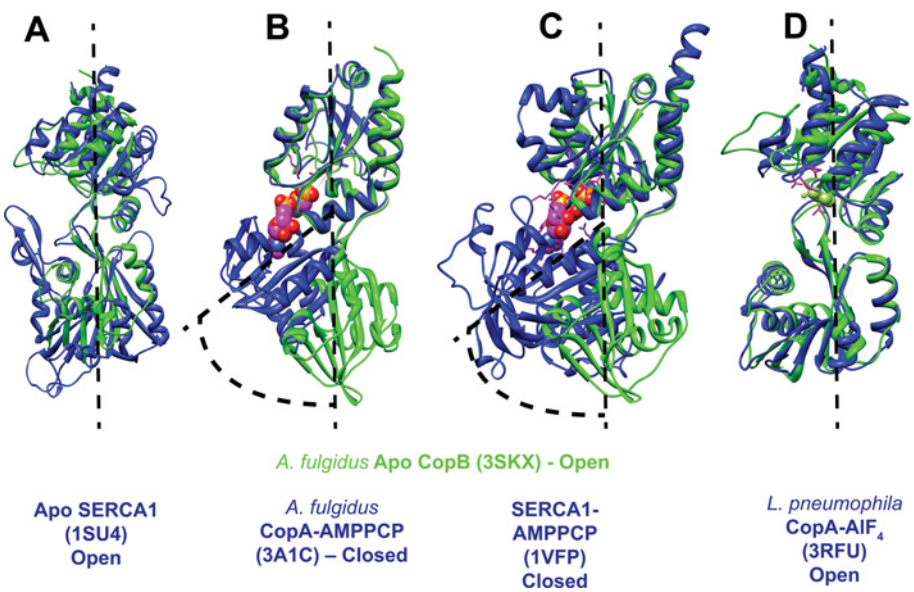

Figure 4 Ribbon representations of superimposed ATPBDs indicating conformational changes

A. fulgidus CopB apo-ATPBD (PDB code 3SKX) (in green) is superimposed with (**A**) Apo SERCA1 (PDB code 1SU4), (**B**) *A. fulgidus* CopA–AMPPCP (PDB code 3A1C), (**C**) SERCA1-AMPPCP (PDB code 1VFP) and (**D**) *L. pneumophila* Lp-CopA, AlF_4 (3RFU). The structural alignment was performed using the structure comparison tool Matchmaker in the program UCSF Chimera. The ribbon diagram was generated using UCSF Chimera.

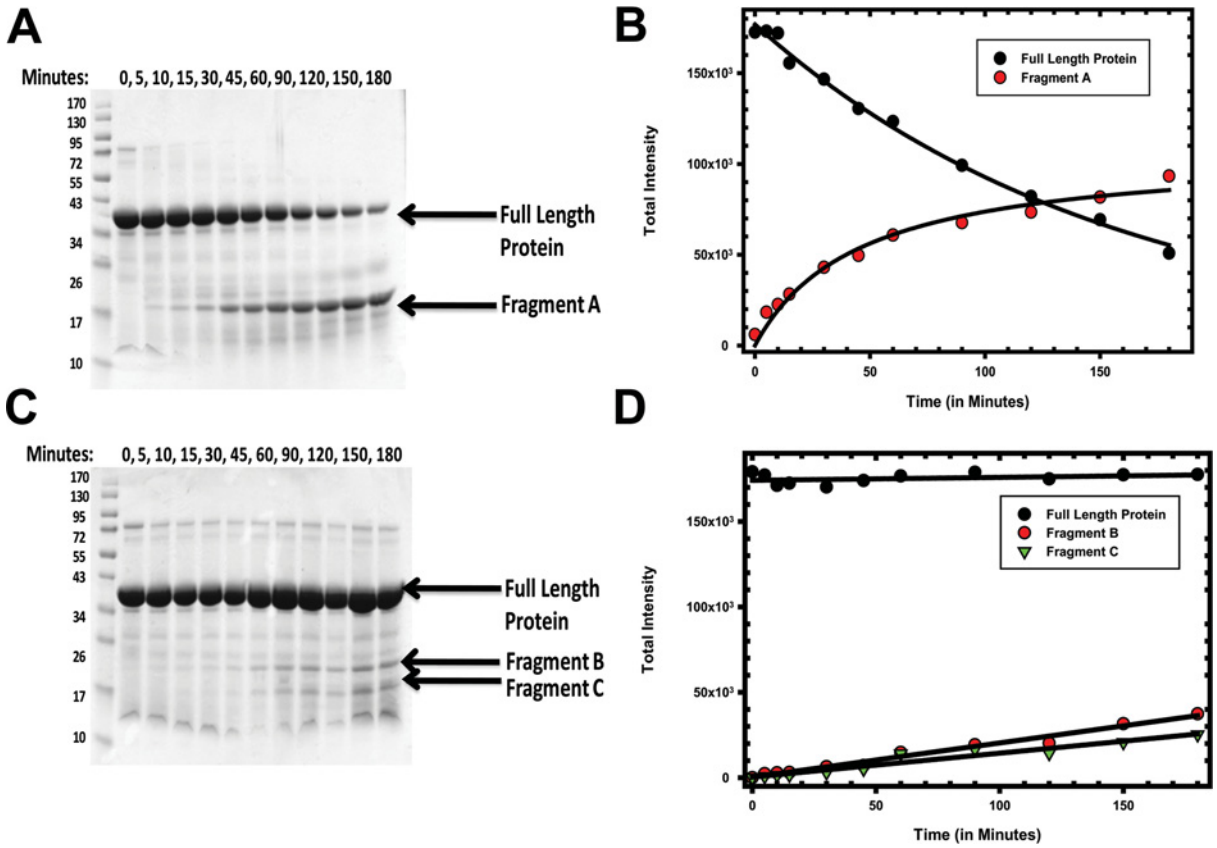

Figure 5 **Limited proteolysis of the ATPBD of *A. fulgidus* CopB**

(**A**) SDS/PAGE gel of the proteolysis reaction performed in the absence of AMPPCP. (**B**) Total intensities of the two prominent bands (full-length protein and Fragment A) in the gel plotted as a function of time. (**C**) SDS/PAGE gel of the reaction performed in the presence of 5 mM AMPPCP. (**D**) Total intensities of the three prominent bands (full-length protein and Fragments B and C).

and the hypothetical hydrogenase from *Enterococcus faecalis* (PDB CODE 1YV9) also binds phosphate in the absence of Mg(II).

Comparing the anion-binding site to other known structures reveals some interesting insights about the co-ordination complex. The *S. solfataricus* CopB structure (2IYE) is bound to SO_4^{2-}, but in this case, the sulfate ion is approximately 5 Å away from the aspartate residue in the DKTGT sequence, which is the site of phosphorylation [24]. The CopB ATPBD is more similar to other P-type ATPases with bound anions, in which the anion occupies a position close to the site of phosphorylation (Supplementary Figure S5 at http://www.bioscirep.org/bsr/032/bsr0320443add.htm). This location supports the proposal that the bound phosphate in the CopB ATPBD is the product after hydrolysis of the covalent aspartyl phosphate bond.

Open and closed conformations

The P- and N-domains of the ATPBD are linked by two extended β-strands that could potentially act as a hinge. The ligand-induced conformational change of the ATPBD caused by the binding and hydrolysis of ATP could be the key to the energy transfer from the active site to the helices (α1 and α10) adjoining the transmembrane helices H6 and H7 [17,42,43]. This region is clearly important for the catalytic cycle because mutations in the highly conserved residues in these regions in the human copper-transporting P-type ATPases result in debilitating hepatic and neurodegenerative diseases [47].

Previously determined structures of ATPBDs have been observed in both open and closed conformations in which the P- and N-domains are reoriented with respect to each other. However, the physiological factors that influence movement of the domains are still under discussion, and in the observed crystal structures it is possible that crystal packing forces have some influence. The CopB apo-ATPBD determined here was found in the open conformation, similar to the apo-SERCA1 structure (PDB code 1SU4) [13] (Figure 4). The open conformation of the apo-state makes sense with the expectation that this conformation would allow access for nucleotide binding. The two ATPBDs that were co-crystallized with non-hydrolysable

nucleotides, *A. fulgidus* CopA–AMPPCP (PDB code 3A1C) [25] and SERCA1–AMPPCP (PDB code 1VFP) [17], were both observed in the closed conformation, suggesting that the P- and N-domains of the ATPBD move to facilitate simultaneous contacts from both domains with the nucleotide (Figure 4). After phosphorylation of the aspartate in the P-domain, the reopening of the P- and N-domains is necessary for the release of ADP. Thus, the open conformation is poised for subsequent product release after dephosphorylation, as we have observed here in the phosphate-bound structure of the CopB ATPBD. The open conformation is also seen in the Lp-CopA structure with the product analogue AlF_4 [29] (Figure 4).

To avoid the potential effects of crystal packing forces on the conformation of the ATPBD, we examined the conformation of the CopB ATPBD in solution using limited proteolysis in the absence and presence of nucleotide. With this approach, differences in the number and/or size of fragments produced from proteolysis reflect the conformation of the different states. After proteolysis of the ATPBD in the absence of AMPPCP, two major species were observed (Figure 5). One species is the full-length protein and the other is a smaller fragment that migrates between the 17 and 26 kDa marker (labelled as fragment A in Figure 5). In the presence of 5 mM AMPPCP, two major proteolysis products were observed (labelled as fragments B and C in Figure 5), both of which are different from the major fragment observed in the apo-state. Furthermore, in the presence of nucleotide the full-length ATPBD predominates during the 3 h course of the experiment, indicating that the rate of proteolysis is significantly decreased when a nucleotide is present. There are two major conclusions from this experiment. Firstly, different cleavage patterns indicate different predominant conformations for the apo- and nucleotide-bound states. Secondly, the decrease in cleavage rate indicates overall stability/rigidity conferred on the protein when bound to AMPPCP. This is the first demonstration of conformational changes of the ATPBD in solution, and supports the hypothesis that the P- and N-domains adopt a closed conformation in the presence of nucleotide.

Ligand-induced conformational changes in solution were also examined by intrinsic Trp^{546} fluorescence experiments. The ATPBD of CopB has one Trp^{546} residue situated in helix $\alpha 7$, which is proximal to the hinge region (Figure 6A). This residue serves as a natural probe for interdomain conformational changes that result from nucleotide binding. The CopB ATPBD exhibits high affinity for ATP ($K_d = 34 \pm 2\ \mu M$) as calculated from the change in fluorescence signal upon the addition of ATP (Supplementary Figure S6 at http://www.bioscirep.org/bsr/032/bsr0320443add.htm). More importantly, addition of ATP to the apo-protein results in a decrease in fluorescence emission (Figure 6B), as would be expected if nucleotide binding results in an increase in solvent accessibility of the Trp^{546} residue in the nucleotide-bound state compared with the apo state. Modelling of the CopB ATPBD in closed conformation shows that Trp^{546} would have a significant increase in accessibility in closed conformation as compared with open conformation (Supplementary Figure S7 and Supplementary Table S1 at http://www.bioscirep.org/bsr/032/bsr0320443add.htm). These observations provide further support that the closed conformation is adopted in solution upon nucleotide binding.

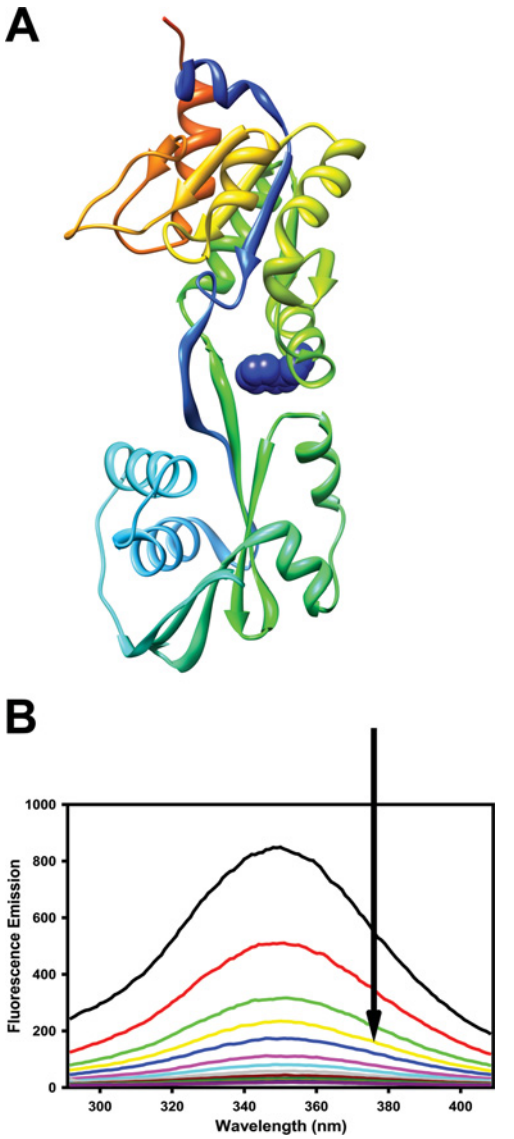

Figure 6 Conformational changes in CopB ATPBD in solution probed by intrinsic tryptophan fluorescence
(**A**) The single tryptophan in the CopB ATPBD, shown in blue space-filling representation, is located proximal to the hinge region. (**B**) Decrease in fluorescence emission at 340 nm accompanies the addition of ATP.

Conclusions

In summary, we report the crystal structures of the apo- and phosphate-bound (Post–E2.Pi) ATPBD of *A. fulgidus* CopB thereby providing a novel structural insight into the catalytic cycle of P-type ATPases. To the best of our knowledge the phosphate-bound structure provides the first glimpse of the ATPBD of a heavy metal ATPase in an open conformation when bound to its physiologically relevant phosphate anion product. Furthermore,

we also report solution studies on the apo- and nucleotide-bound states of the domain revealing that the ATPBD domain adopts different conformations depending on the ligand occupancy, such that it remains open in the apo state to allow ligand binding, closes upon nucleotide binding, and reopens to allow product release. Information about these states helps complete our understanding of the catalytic cycle performed by these ubiquitous ATPases.

AUTHOR CONTRIBUTION

Megan McEvoy designed the research, provided oversight for the experiments, analysis and writing of the paper prior to submission. José Argüello provided oversight for the experiments. Samuel Jayakanthan performed all the experiments, analysed the data and wrote the paper. Sue Roberts and Andrzej Weichsel provided guidance in the MAD and native data collection and structure determination.

ACKNOWLEDGEMENTS

Portions of this research were carried out at the Stanford Synchrotron Radiation Laboratory, a national user facility operated by Stanford University on behalf of the U.S. Department of Energy, Office of Basic Energy Sciences. The SSRL Structural Molecular Biology Program is supported by the Department of Energy, Office of Biological and Environmental Research and by the National Institutes of Health, National Center for Research Resources, Biomedical Technology Program, and the National Institute of General Medical Sciences. We thank Professor Svetlana Lutsenko, Zak Campbell and Yuta Hatori for critical reading of the paper prior to submission.

FUNDING

This work was supported by the National Science Foundation [grant number MCB-0743901 (to J.M.A.)] and the National Institutes of Health [grant number GM079192 (to M.M.M.)].

REFERENCES

1 Moller, J. V., Juul, B. and le Maire, M. (1996) Structural organization, ion transport, and energy transduction of P-type ATPases. Biochim. Biophys. Acta **1286**, 1–51
2 Lutsenko, S. and Kaplan, J. H. (1995) Organization of P-type ATPases: significance of structural diversity. Biochemistry **34**, 15607–15613
3 Axelsen, K. B. and Palmgren, M. G. (1998) Evolution of substrate specificities in the P-type ATPase superfamily. J. Mol. Evol. **46**, 84–101
4 Arguello, J. M., Eren, E. and Gonzalez-Guerrero, M. (2007) The structure and function of heavy metal transport P1B-ATPases. Biometals **20**, 233–248
5 Solioz, M. and Vulpe, C. (1996) CPx-type ATPases: a class of P-type ATPases that pump heavy metals. Trends Biochem. Sci. **21**, 237–241
6 Williams, L. E. and Mills, R. F. (2005) P_{1B}-ATPases – an ancient family of transition metal pumps with diverse functions in plants. Trends Plant Sci. **10**, 491–502
7 De Hertogh, B., Lantin, A. C., Baret, P. V. and Goffeau, A. (2004) The archaeal P-type ATPases. J. Bioenerg. Biomembr. **36**, 135–142
8 Mandal, A. K., Cheung, W. D. and Arguello, J. M. (2002) Characterization of a thermophilic P-type Ag^+/Cu^+-ATPase from the extremophile *Archaeoglobus fulgidus*. J. Biol. Chem. **277**, 7201–7208
9 Mana-Capelli, S., Mandal, A. K. and Arguello, J. M. (2003) *Archaeoglobus fulgidus* CopB is a thermophilic Cu^{2+}-ATPase: functional role of its histidine-rich-N-terminal metal binding domain. J. Biol. Chem. **278**, 40534–40541
10 Bull, P. C., Thomas, G. R., Rommens, J. M., Forbes, J. R. and Cox, D. W. (1993) The Wilson disease gene is a putative copper transporting P-type ATPase similar to the Menkes gene. Nat. Genet. **5**, 327–337
11 Vulpe, C., Levinson, B., Whitney, S., Packman, S. and Gitschier, J. (1993) Isolation of a candidate gene for Menkes disease and evidence that it encodes a copper-transporting ATPase. Nat. Genet. **3**, 7–13
12 Bull, P. C. and Cox, D. W. (1994) Wilson disease and Menkes disease: new handles on heavy-metal transport. Trends Genet. **10**, 246–252
13 Toyoshima, C., Nakasako, M., Nomura, H. and Ogawa, H. (2000) Crystal structure of the calcium pump of sarcoplasmic reticulum at 2.6 Å resolution. Nature **405**, 647–655
14 Barry, A. N., Shinde, U. and Lutsenko, S. (2010) Structural organization of human Cu-transporting ATPases: learning from building blocks. J. Biol. Inorg. Chem. **15**, 47–59
15 Mandal, A. K. and Arguello, J. M. (2003) Functional roles of metal binding domains of the *Archaeoglobus fulgidus* Cu^+-ATPase CopA. Biochemistry **42**, 11040–11047
16 Agarwal, S., Hong, D., Desai, N. K., Sazinsky, M. H., Arguello, J. M. and Rosenzweig, A. C. (2010) Structure and interactions of the C-terminal metal binding domain of *Archaeoglobus fulgidus* CopA. Proteins **78**, 2450–2458
17 Toyoshima, C. and Mizutani, T. (2004) Crystal structure of the calcium pump with a bound ATP analogue. Nature **430**, 529–535
18 Moller, J. V., Lenoir, G., Marchand, C., Montigny, C., le Maire, M., Toyoshima, C., Juul, B. S. and Champeil, P. (2002) Calcium transport by sarcoplasmic reticulum Ca^{2+}-ATPase. Role of the A domain and its C-terminal link with the transmembrane region. J. Biol. Chem. **277**, 38647–38659
19 Pedersen, B. P., Buch-Pedersen, M. J., Morth, J. P., Palmgren, M. G. and Nissen, P. (2007) Crystal structure of the plasma membrane proton pump. Nature **450**, 1111–1114
20 Morth, J. P., Pedersen, B. P., Toustrup-Jensen, M. S., Sorensen, T. L., Petersen, J., Andersen, J. P., Vilsen, B. and Nissen, P. (2007) Crystal structure of the sodium-potassium pump. Nature **450**, 1043–1049
21 Bublitz, M., Poulsen, H., Morth, J. P. and Nissen, P. (2010) In and out of the cation pumps: P-type ATPase structure revisited. Curr. Opin. Struct. Biol. **20**, 431–439
22 Bublitz, M., Morth, J. P. and Nissen, P. (2011) P-type ATPases at a glance. J. Cell Sci. **124**, 2515–2519
23 Tsivkovskii, R., MacArthur, B. C. and Lutsenko, S. (2001) The Lys1010–Lys1325 fragment of the Wilson's disease protein binds nucleotides and interacts with the N-terminal domain of this protein in a copper-dependent manner. J. Biol. Chem. **276**, 2234–2242
24 Lubben, M., Guldenhaupt, J., Zoltner, M., Deigweiher, K., Haebel, P., Urbanke, C. and Scheidig, A. J. (2007) Sulfate acts as phosphate analog on the monomeric catalytic fragment of the CPx-ATPase CopB from *Sulfolobus solfataricus*. J. Mol. Biol. **369**, 368–385
25 Sazinsky, M. H., Mandal, A. K., Arguello, J. M. and Rosenzweig, A. C. (2006) Structure of the ATP binding domain from the *Archaeoglobus fulgidus* Cu^+-ATPase. J. Biol. Chem. **281**, 11161–11166

26 Dmitriev, O. Y., Bhattacharjee, A., Nokhrin, S., Uhlemann, E. M. and Lutsenko, S. (2011) Difference in stability of the N-domain underlies distinct intracellular properties of the E1064A and H1069Q mutants of copper-transporting ATPase ATP7B. J. Biol. Chem. **286**, 16355–16362
27 Dmitriev, O., Tsivkovskii, R., Abildgaard, F., Morgan, C. T., Markley, J. L. and Lutsenko, S. (2006) Solution structure of the N-domain of Wilson disease protein: distinct nucleotide-binding environment and effects of disease mutations. Proc. Natl. Acad. Sci. U.S.A. **103**, 5302–5307
28 Tsuda, T. and Toyoshima, C. (2009) Nucleotide recognition by CopA, a Cu^{+}-transporting P-type ATPase. EMBO J. **28**, 1782–1791
29 Gourdon, P., Liu, X. Y., Skjorringe, T., Morth, J. P., Moller, L. B., Pedersen, B. P. and Nissen, P. (2011) Crystal structure of a copper-transporting PIB-type ATPase. Nature **475**, 59–64
30 Pflugrath, J. W. (1999) The finer things in X-ray diffraction data collection. Acta Crystallogr. D Biol. Crystallogr. **55**, 1718–1725
31 Terwilliger, T. (2004) SOLVE and RESOLVE: automated structure solution, density modification and model building. J. Synchrotron Radiat. **11**, 49–52
32 Cowtan, K. (2006) The Buccaneer software for automated model building. 1. Tracing protein chains. Acta Crystallogr. D Biol. Crystallogr. **62**, 1002–1011
33 Murshudov, G. N., Vagin, A. A. and Dodson, E. J. (1997) Refinement of macromolecular structures by the maximum-likelihood method. Acta Crystallogr. D Biol. Crystallogr. **53**, 240–255
34 Emsley, P., Lohkamp, B., Scott, W. G. and Cowtan, K. (2010) Features and development of Coot. Acta Crystallogr. D Biol. Crystallogr. **66**, 486–501
35 Kornbrot, D. (2000) Statistical software for microcomputers: SigmaPlot 2000 and SigmaStat2. Br. J. Math. Stat. Psychol. **53**, 335–337
36 Arnold, K., Bordoli, L., Kopp, J. and Schwede, T. (2006) The SWISS-MODEL workspace: a web-based environment for protein structure homology modelling. Bioinformatics **22**, 195–201
37 Collaborative Computational Project, Number 4 (1994) The CCP4 suite: programs for protein crystallography. Acta Crystallogr. D Biol. Crystallogr. **50**, 760–763
38 Ballal, A., Basu, B. and Apte, S. K. (2007) The Kdp-ATPase system and its regulation. J. Biosci. **32**, 559–568
39 Altendorf, K., Gassel, M., Puppe, W., Mollenkamp, T., Zeeck, A., Boddien, C., Fendler, K., Bamberg, E. and Drose, S. (1998) Structure and function of the Kdp-ATPase of *Escherichia coli*. Acta Physiol. Scand. Suppl. **643**, 137–146
40 Orengo, C. A., Michie, A. D., Jones, S., Jones, D. T., Swindells, M. B. and Thornton, J. M. (1997) CATH – a hierarchic classification of protein domain structures. Structure **5**, 1093–1108
41 Burroughs, A. M., Allen, K. N., Dunaway-Mariano, D. and Aravind, L. (2006) Evolutionary genomics of the HAD superfamily: understanding the structural adaptations and catalytic diversity in a superfamily of phosphoesterases and allied enzymes. J. Mol. Biol. **361**, 1003–1034
42 Sorensen, T. L., Moller, J. V. and Nissen, P. (2004) Phosphoryl transfer and calcium ion occlusion in the calcium pump. Science **304**, 1672–1675
43 Toyoshima, C., Nomura, H. and Tsuda, T. (2004) Lumenal gating mechanism revealed in calcium pump crystal structures with phosphate analogues. Nature **432**, 361–368
44 Moncoq, K., Trieber, C. A. and Young, H. S. (2007) The molecular basis for cyclopiazonic acid inhibition of the sarcoplasmic reticulum calcium pump. J. Biol. Chem. **282**, 9748–9757
45 Olesen, C., Sorensen, T. L., Nielsen, R. C., Moller, J. V. and Nissen, P. (2004) Dephosphorylation of the calcium pump coupled to counterion occlusion. Science **306**, 2251–2255
46 Fieulaine, S., Lunn, J. E., Borel, F. and Ferrer, J. L. (2005) The structure of a cyanobacterial sucrose-phosphatase reveals the sugar tongs that release free sucrose in the cell. Plant Cell **17**, 2049–2058
47 Linz, R. and Lutsenko, S. (2007) Copper-transporting ATPases ATP7A and ATP7B: cousins, not twins. J. Bioenerg. Biomembr. **39**, 403–407
48 Pettersen, E. F., Goddard, T. D., Huang, C. C., Couch, G. S., Greenblatt, D. M., Meng, E. C. and Ferrin, T. E. (2004) UCSF Chimera – a visualization system for exploratory research and analysis. J. Comput. Chem. **25**, 1605–1612
49 Thompson, J. D., Higgins, D. G. and Gibson, T. J. (1994) CLUSTAL W: improving the sensitivity of progressive multiple sequence alignment through sequence weighting, position-specific gap penalties and weight matrix choice. Nucleic Acids Res. **22**, 4673–4680
50 Gouet, P., Courcelle, E., Stuart, D. I. and Metoz, F. (1999) ESPript: analysis of multiple sequence alignments in PostScript. Bioinformatics **15**, 305–308

Received 16 May 2012; accepted 25 May 2012
Published as Immediate Publication 4 June 2012, doi 10.1042/BSR20120048

Biosci. Rep. (2012) / **32** / 443–453 (Printed in Great Britain) / doi 10.1042/BSR20120048

online data

Original Paper

SUPPLEMENTARY ONLINE DATA

Conformations of the apo-, substrate-bound and phosphate-bound ATP-binding domain of the Cu(II) ATPase CopB illustrate coupling of domain movement to the catalytic cycle

Samuel JAYAKANTHAN*, Sue A. ROBERTS*, Andrzej WEICHSEL*, José M. ARGÜELLO† and Megan M. McEVOY*‡[1]

*Department of Chemistry and Biochemistry, University of Arizona, Tucson, AZ 85721, U.S.A., ‡Department of Soil, Water and Environmental Science, University of Arizona, Tucson, AZ 85721, U.S.A., and †Department of Chemistry and Biochemistry, Worcester Polytechnic Institute, 100 Institute Road, Worcester, MA 01609, U.S.A.

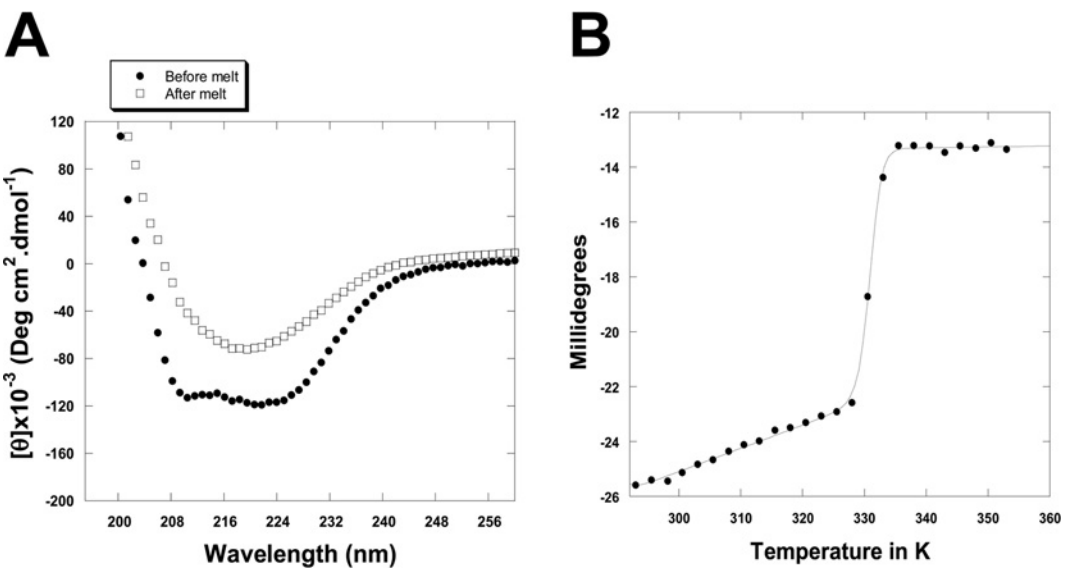

Figure S1 **Far-UV CD Spectra of the ATPBD**

(**A**) Far-UV CD spectra of ATPBD before (closed circles) and after (open squares) the temperature melt. (**B**) Loss of signal at 222 nm upon an increase in temperature indicates unfolding of the ATPBD. The midpoint of the transition (T_m) is 60 °C.

[1] To whom correspondence should be addressed at the present address: Department of Chemistry and Biochemistry, University of Arizona, Tucson, AZ 85721, U.S.A. (email mcevoy@email.arizona.edu).

The atomic co-ordinates and the structure factors of the apo- and phosphate-bound ATPBD of *Archaeoglobus fulgidus* CopB crystallized in space group $P22_12_1$ will appear in the PDB under accession codes 3SKX and 3SKY respectively.

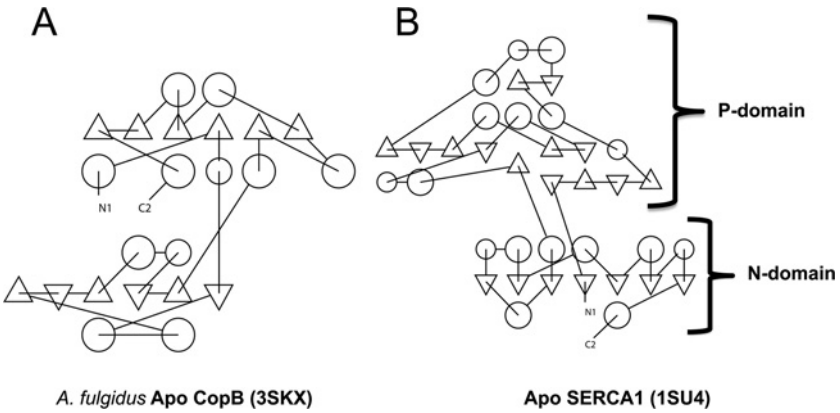

Figure S2 TOPS cartoon depicting the ATPBDs of (A) *A. fulgidus* CopB (PDB code 3SKX) and (B) SERCA1 (PDB code 1SU4) in two-dimensional representation

Helices are depicted as circles and strands are depicted as triangles. Cartoons were generated using the TOPS algorithm.

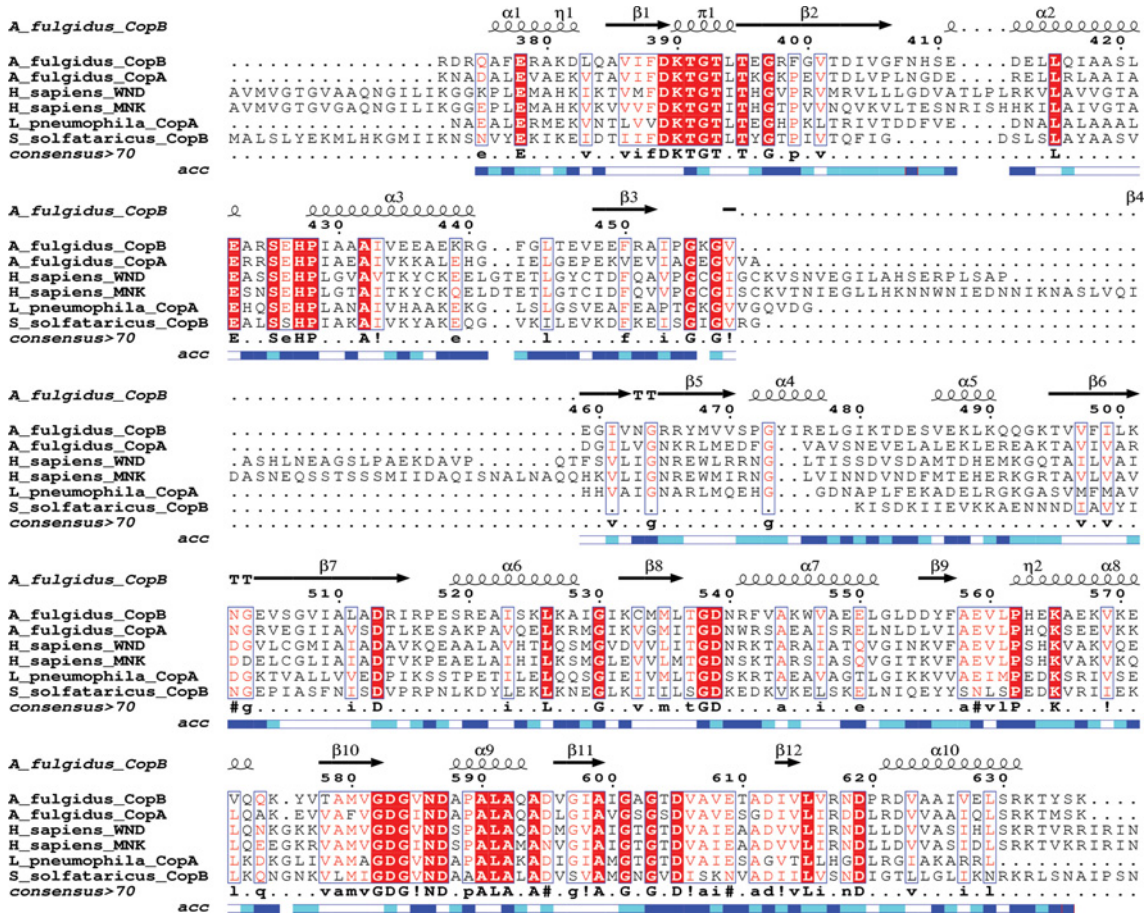

Figure S3 **Multiple sequence alignment of the ATPBDs of six ATPases including *A. fulgidus* CopB**
The alignment contains sequences of CopA and CopB from *A. fulgidus*, CopB from *S. solfataricus,* CopA from *L. pnuemophila,* human Cu-ATPases ATP7A and ATP7B (also termed as MNK and WND from *H. sapiens*). Sequence alignment was performed using CLUSTALW [1]. Secondary structural elements along with numbering for *A. fulgidus* CopB are drawn on top of the entire alignment. The solvent accessible residues are indicated by a bar running parallel to the alignment with colors ranging from white to dark blue. The accessibility information is extracted from the corresponding DSSP file. Blue indicates accessible, cyan indicates intermediate, and white indicates that the residues are buried. The entire Figure was prepared using the program ESPript [2].

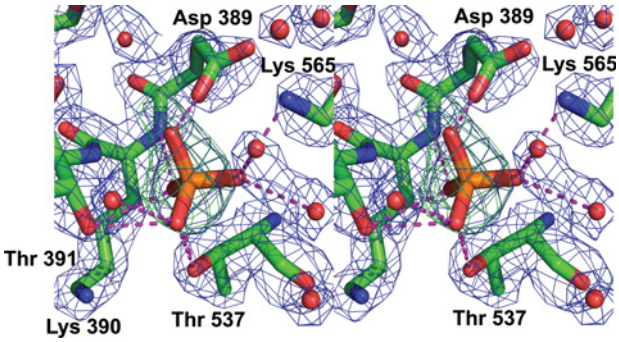

Figure S4 Phosphate-binding site in the P-domain
A stereo view of the electron density map of the anion-binding pocket after final refinement is shown. The $2|F_o–F_c|$ weighted electron density omit map (shown in blue) is contoured to 1.5σ. This map was calculated after final refinement of the 2.1 Å data removing the phosphate anion from the active site and refined using REFMAC. The difference electron density map $1|F_o–F_c|$ of the deleted phosphate (P_i) anion is shown in green. The water molecules are shown as red spheres. The dashed lines (magenta) indicate hydrogen bonds and salt bridges. The maps were calculated using CCP4i, and the final Figure was generated using PyMOL.

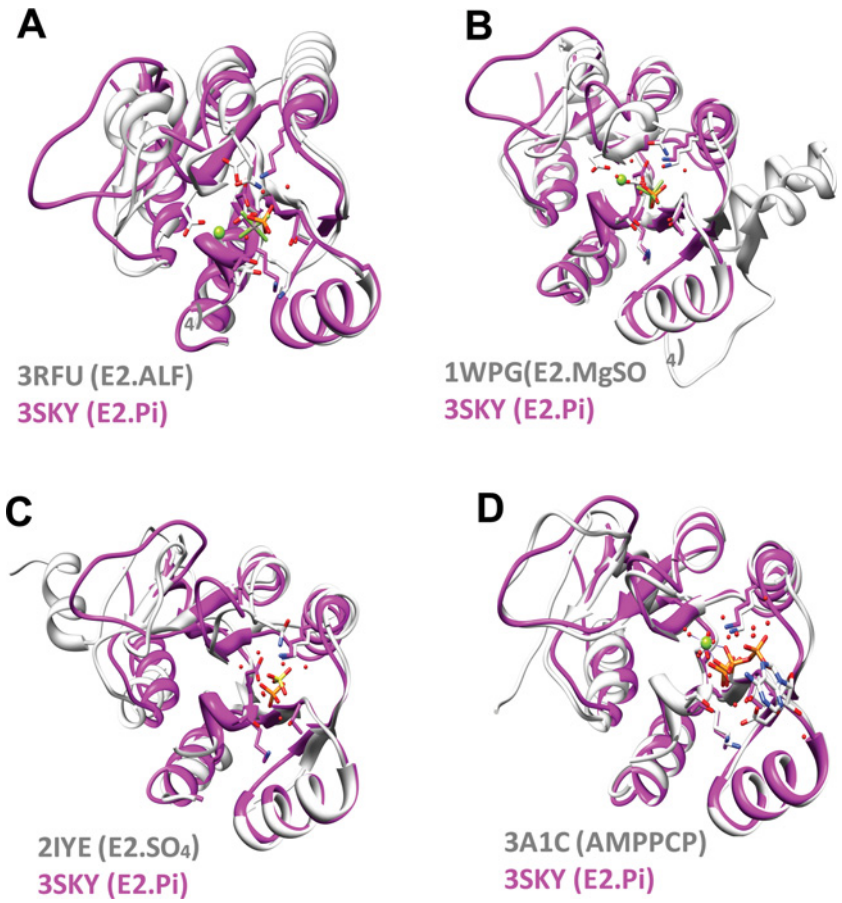

Figure S5 **Superposition of the P-domain of the phosphate-bound structure of *A. fulgidus* CopB with that of related P-type ATPases with bound anion or nucleotide**

The P-domain of *A. fulgidus* CopB (PDB code 3SKY) is shown as a purple ribbon diagram and the other ATPases are shown as grey ribbon models. The phosphate anion is represented in an orange stick model with surrounding water molecules as red spheres. Magnesium ions are represented as green spheres. (**A**) CopA from L. *pneumophila*. The AlF_4 transition state mimic is represented as a green stick. (**B**) Ca(II) ATPase SERCA1 (PDB code 1WPG). The $MgSO_4$ is shown in green. (**C**) CopB from *S. solfataricus* (PDB code 2IYE). The SO_4 anion is shown in yellow. (**D**) CopA from *A. fulgidus*. The bound nucleotide (AMPPCP) with its γ-phosphate group is shown as white, blue, orange and red sticks. Models were generated using UCSF Chimera.

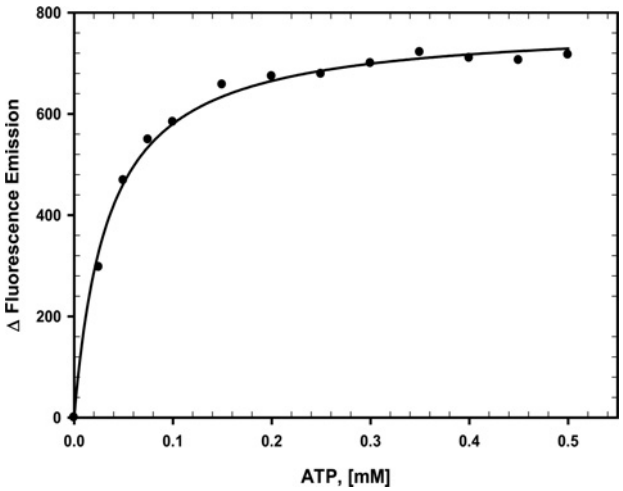

Figure S6 Change in fluorescence emission plotted as function of ATP concentration
Fitting to a single site-binding model results in a K_d of 34±2 μM.

Table S1 Solvent accessible surface area for Trp^{546} calculated using the program AREAIMOL

	van der Waals radii (Å)	
Atom name (Trp^{546})	**Open conformation (PDB code 3SKX)**	**Closed conformation [modelled from CopA (PDB code 3A1C)]**
N	0.2	0.3
CA	2.1	0.7
C	0	0
O	0	0
CB	0.7	0
CG	0	0
CD1	3.8	0.5
CD2	0	0
NE1	2.2	8.4
CE2	0	0
CE3	0.9	1.4
CZ2	11.6	28.9
CZ3	0.6	12.1
CH2	1.3	29.9

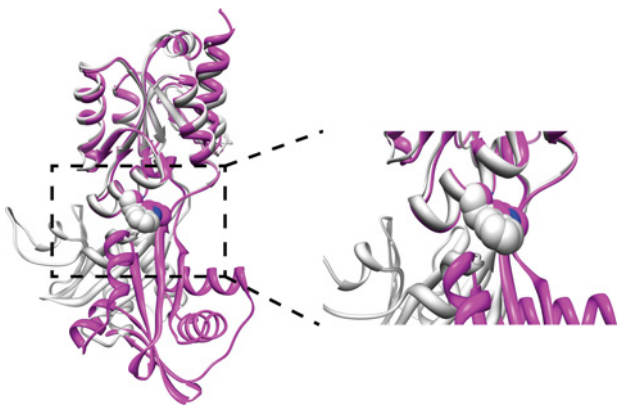

Figure S7 Overlay of apo CopB (open conformation, purple ribbon) with the homology model of CopB (closed conformation, grey ribbon)
Trp^{546} is shown in space-filling representation in both models. The solvent accessibility of the tryptophan side chain increases in the closed conformation. The van der Waals radii of the atoms in the tryptophan residue in the open and closed conformations are reported in Supplementary Table S1.

REFERENCES

1 Thompson, J. D., Higgins, D. G. and Gibson, T. J. (1994) CLUSTALW: improving the sensitivity of progressive multiple sequence alignment through sequence weighting, position-specific gap penalties and weight matrix choice. Nucleic Acids Res. **22**, 4673–4680
2 Gouet, P., Courcelle, E., Stuart, D. I. and Metoz, F. (1999) ESPript: analysis of multiple sequence alignments in PostScript. Bioinformatics **15**, 305–308

Received 16 May 2012; accepted 25 May 2012
Published as Immediate Publication 4 June 2012, doi 10.1042/BSR20120048